The Evolution of Flare Activity with Stellar Age

James. R. A. Davenport,[1,2,*] Kevin R. Covey,[1] Riley W. Clarke,[1] Austin C. Boeck,[1]
Jonathan Cornet,[1] and Suzanne L. Hawley[2]

[1]Department of Physics & Astronomy, Western Washington University, 516 High St., Bellingham, WA 98225, USA
[2]Department of Astronomy, University of Washington, Seattle, WA 98195, USA

ABSTRACT

Using a recent census of flare stars from the *Kepler* survey, we have explored how flare activity evolves across stellar main sequences lifetimes. We utilize a sample of 347 stars with robust flare activity detections, and which have rotation periods measured via starspot modulations in their *Kepler* light curves. To measure these change in activity over time, we have described in detail the benefits and challenges of using three separate methods for quantifying flare activity from optical light curves. These metrics include: the fractional luminosity emitted in flares, the specific rate of flares emitted at a given energy, and a model for the entire flare frequency distribution. With all three approaches we find that flare activity decreases for all low-mass stars as they spin-down, and thus with age. Most striking is the change in flare occurrence frequency distributions, which show no significant change in the power law slope with age. Since our sample is preferentially constructed of younger, more active stars, our model over-predicts the super-flare rate previously estimated for the Sun. Our best-fit model of this evolution in the flare frequency distribution is parameterized for ease of use by other researchers as a function of stellar mass and age.

1. INTRODUCTION

Surface magnetic activity is observed to decline over time for low-mass stars on the main sequence. Magnetic activity comes in a wide range of observable phenomena, including UV and X-ray luminosity, cool starspots, and flares. As the star loses angular momentum via stellar winds, the rotation velocity decreases and the internal magnetic dynamo is quieted. This age–activity connection was outlined in the seminal work by Skumanich (1972), which has been

Corresponding author: James. R. A. Davenport
James.Davenport@wwu.edu

* NSF Astronomy and Astrophysics Postdoctoral Fellow
DIRAC Fellow

directly connected with flare activity as well (Skumanich 1986). Magnetic activity evolution has been confirmed for low-mass stars (late F through early M type) in many studies using X-ray luminosity (Wright et al. 2011), UV emission (Shkolnik & Barman 2014), Zeeman-Doppler imaging (Vidotto et al. 2014), and Hα emission (West et al. 2015), to name but a few.

This surface activity can have significant impact on the evolution of habitable zone planets orbiting active stars. Flares in particular have been studied as a possible threat to a planet's ability to retain a habitable atmosphere (e.g. Segura et al. 2010; Luger et al. 2015; Tilley et al. 2017). For example, UV flux and high energy particles impacting a terrestrial planet's atmosphere from frequent stellar flares can signifi-

cantly deplete ozone, and result in a potentially uninhabitable planetary surface (Tilley et al. 2017). Under more extreme scenarios, stellar activity could strip large portions of a planet's atmosphere away over timescales of a few 100 Myr (Luger et al. 2015). The duration of high flare activity early in a star's life may therefore be a fundamental property in defining potential planetary habitability.

Stellar activity also makes planet searches more difficult, adding both slow variability (e.g. starspots) that can impact radial velocity studies, and fast stochastic variability (e.g. flares) that can impede transit searches (e.g. Kipping et al. 2017). Further, though stellar activity is less prominent at redder wavelengths, even observing in the infrared does not eliminate the potential for flares from active stars to impact transit searches, particularly for the lowest mass stars (Davenport 2017a). To understand planet occurrence rates for nearby low-mass stars, as well as the evolution of planetary habitability, we must constrain flare rates and properties as a function of stellar age.

Measuring the evolution of flare activity with stellar age has typically been limited to comparisons between flare stars in young clusters or stellar associations with known ages. Studying flare stars in young nearby moving groups and clusters reaches back at least five decades (Haro & Chavira 1966), with the conclusion that all low-mass dwarf stars undergo an evolution in flare activity (Ambartsumian & Mirzoian 1975). Pre-main sequence stars have also been known to exhibit high levels of flare activity compared to field-aged dwarfs (e.g. Feigelson 2001). However, in most previous studies field stars are assumed to be approximately Solar-aged, and therefore generally flare-inactive, since few reliable age indicators for isolated field stars exist.

Space-based exoplanet transit missions such as Kepler (Borucki et al. 2010) have provided a revolutionary dataset for statistical stud-ies of flare stars, particularly for field dwarfs (Walkowicz et al. 2011). Such missions are ideally suited for large scale studies of flares, as they produce high precision, continuous light curves for months to years in duration. The Kepler survey has been used to explore "super-flare" activity (events with energies more than 10 times larger than those observed on the Sun) from solar-mass stars (Shibayama et al. 2013), as well as from K and M dwarfs (Candelaresi et al. 2014). White-light flares in Kepler light curves have been detected across the main sequence, from massive A and F stars (Balona 2012) down to L dwarfs (Gizis et al. 2013), and produced the most detailed catalogs of flares for individual active stars to date (Hawley et al. 2014; Davenport et al. 2014a).

In this paper we present an ensemble analysis of flare activity in the Kepler field, based on the flare sample amassed in Davenport (2016b). This sample was generated using an automated processing of the entire Kepler light curve database, and produced a sample of over 4000 candidate flare stars. The Davenport (2016b) catalog of flares provides the most complete census of flare activity from a large sample of field stars to date, and is the ideal dataset to study the evolution of flare rates with stellar age.

Here we explore the relationship between flare occurrence rates and stellar ages (derived from rotation periods) for stars in the Kepler field. Our sample of flare stars with measured rotation periods is detailed in §2. We present three approaches for quantitatively tracing changes in flare activity over time, including modeling the flare frequency distribution as a function of both stellar mass and age in §3. In §4 we explore the empirical evolution of flare activity for our Kepler sample, and provide an analytic prescription for use in other studies. Finally, a short discussion and comparison to other studies is given in §5.

2. FLARE STAR SAMPLE

Our sample of flare stars comes from the automated search of *Kepler* light curves from Davenport (2016b). This study produced the most comprehensive analysis of the *Kepler* field for stellar flares, processing every short (1-minute) and long (30-minute) cadence light curve in search of flares. Davenport (2016b) produced an open-source Python flare analysis codebase named `appaloosa`, designed to detrend (model) *Kepler* light curves of both instrumental and astrophysical noise, detect flare candidates (positive, significant outliers), and determine the reliability of the detected flares via artificial flare injection and recovery tests. These completeness tests were run on each continuous local segment of light curve available for every star, resulting in variable completeness limits for each star as the light curve noise properties change. Davenport (2016b) made both the `appaloosa` code, and the code to generate the figures and results in the paper available online. The results presented in this paper directly extend the work of Davenport (2016b), and so we also make our analysis code available as an update to the `appaloosa` project online.[1]

2.1. *Selecting a Robust Sample*

Since we are focused here on quantifying the changes of flare activity with stellar age, we limit our analysis to stars with measured rotation periods so that stellar rotation periods can be used as a proxy for age. We note that while the rotation–age connection may be more complex than most gyrochronology prescriptions, e.g. the weakened rotational braking found in Solar-age stars from van Saders et al. (2016), rotation nonetheless increases continuously with age (i.e. stars nominally do not speed up while on the main sequence). Rotation is therefore a good means to *sort* stars by their age, even

if the specific age derived from gyrochronology relations is not accurate. Our work here is further insulated from these effects, as the sample of flare star candidates from Davenport (2016b) predominantly have rotation ages of $\lesssim 1$ Gyr. We specifically adopt for our analysis the rotation period catalog of McQuillan et al. (2014), which derived 34,040 periods from *Kepler* data using the Autocorrelation Function, and did extensive testing against other period-finding approaches such as the Lomb-Scargle Periodogram.

The Davenport (2016b) sample of $\sim$4,000 candidate flare stars contains several types of contamination from variable stars that do not exhibit flaring activity. For example, we found some eclipsing binaries and pulsating stars were able to fool the `appaloosa` code, due to sharp features in their light curve, particularly at the 30-minute cadence. The worst cases of this failure appear to be caused by insufficient modeling of periodic signals by `appaloosa`, namely by using too few sine curves to fit each significant period found and leaving sharp or peaky structures in the model residuals. Future versions of `appaloosa` will improve on this detrending algorithm, and we urge caution when adopting the Davenport (2016b) flare sample blindly. Our analysis is largely free from such contamination, as we require each star to have an identified rotation period by McQuillan et al. (2014), who rejected such eclipsing and pulsating targets.

In Figure 1 we show light curves and cumulative flare frequency distributions (FFDs) for three example flare stars from the Davenport (2016b) sample that also have rotation periods measured in McQuillan et al. (2014). These example stars will be followed through the analysis of this paper, and were selected to demonstrate a range of flare rates and rotation periods. Each star in the Davenport (2016b) sample required that, within all available *Kepler* data, the star have at least 100 candidate flares of

---
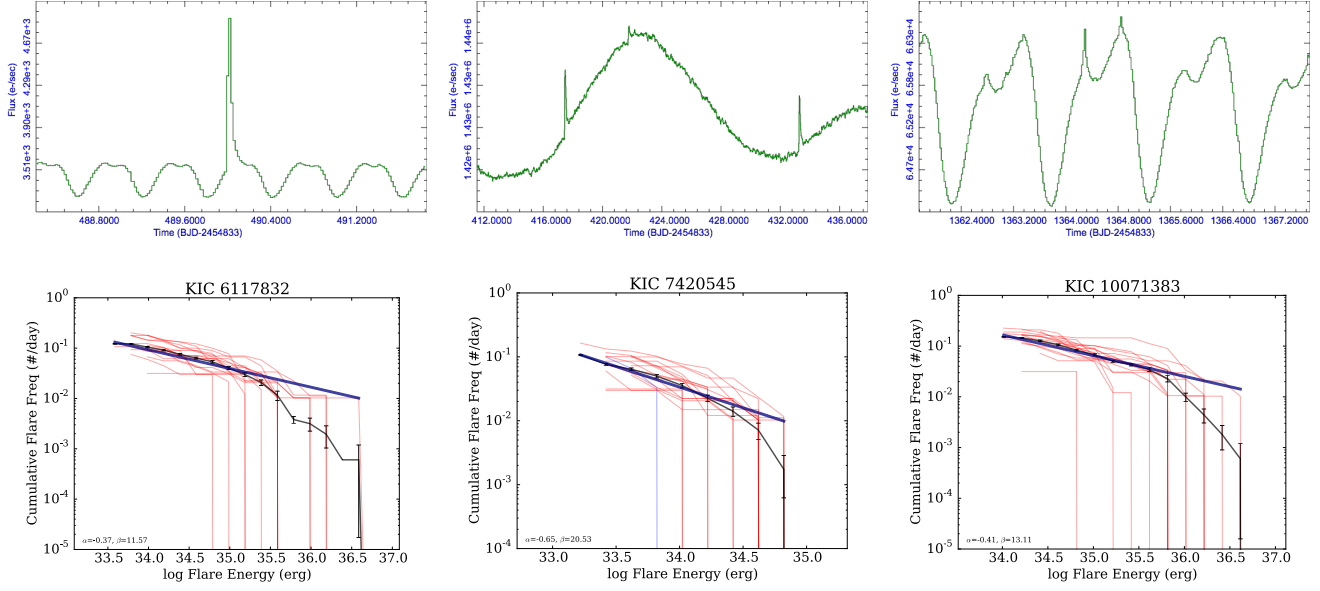
[1] https://github.com/jradavenport/appaloosa

Figure 1. Three examples of flare stars from the Davenport (2016b) sample. top row: sample light curves. Bottom row: cumulative flare frequency distributions (FFDs) from the appaloosa flare finding analysis of Davenport (2016b) for the same three stars. The FFD from each short cadence (blue lines) and long cadence (red lines) dataset is included, as well as the mean FFD (black) with Poisson uncertainties shown. Each star's mean FFD is fit with a power law (heavy navy line), whose slope and intercept in log–log space (α and β) are noted.

any energy, and 10 flares with energies above the 68% completeness threshold determined by the automated flare injection tests be recovered. These conservative thresholds potentially eliminate real flare stars with fewer significant flare events from our analysis, as noted by Van Doorsselaere et al. (2017), and may bias our sample towards the more active (younger) end. In total we study the flare rate evolution from 347 stars with rotation periods from McQuillan et al. (2014) that pass the Davenport (2016b) selection criteria of having sufficient numbers of recovered flare event candidates. We use this conservatively selected, robust sub-sample of 347 stars from the Davenport (2016b) catalog throughout this paper to explore in detail various approaches to quantifying and comparing flare activity .

2.2. *Flare Stars Among the Kepler Field*

The thresholds for flare star selection from Davenport (2016b) can be relaxed to include a larger sample of stars, and to better study the incidence of flare activity in the population of *Kepler* field stars. As a demonstration of this, in Figure 2 we show the fraction of flaring stars found in six bins of $g - i$ color as a function of their gyrochronology age. In this example we analyzed 27,127 stars from McQuillan et al. (2014) that had rotation periods between 0.1 and 30 days, and colors redder than $g - i \geq 0.5$ mag. Stars were considered "active" here if they had at least 3 flare events above the 68% completeness threshold determined by the automated flare injection tests from Davenport (2016b), and had no requirement for the total number of flare event candidates. This figure emulates the Hα activity fraction work typically done for M dwarfs, which shows an increasing lifetime of magnetic activity for stars with decreasing mass (e.g. West et al. 2008). Previous studies such as Kowalski et al. (2009) and Hilton et al. (2010) have explored the fraction of flaring M dwarfs as a function of their height above

the Galactic disk (a dynamical proxy for age), and have found flare activity decreases at earlier ages than Hα emission activity.

The lower mass (redder) stars in Figure 2 exhibit both a higher overall fraction of flare activity at all ages, and a qualitatively longer lifetime of flare activity. Note this sample has not been cleared of contaminants from e.g. subgiants, which have been shown by Davenport (2017b) to significantly contaminate the rotating G dwarf sample from McQuillan et al. (2014), and which may lower the overall flaring fraction for bluer stars plotted here. A more detailed census of stellar rotation periods and ages for all *Kepler* and K2 stars (e.g. see van Saders et al. 2018), as well as an exploration on the robustness of identifying flare stars from small numbers of events is needed to fully understand these flare activity lifetimes. Still, we believe this is the first demonstration of flare activity lifetimes for G, K, and M field dwarfs together, and warrants further study.

3. QUANTIFYING FLARE ACTIVITY

In order to accurately measure the evolution of flare rates over time, we must find a suitable metric to characterize flare activity for an ensemble of stars. Typical magnetic activity indicators, such as Hα or X-ray flux, are used as disk-integrated measures of magnetically-driven emission from the chromosphere or corona. These quantities are are often presented as relative luminosities, normalized either to a continuum flux, or to the stellar bolometric luminosity. While the overall rate and maximum intensity of flares for a given star are related to the global magnetic field strength, the specific properties of individual flare events (e.g. duration, amplitude, morphology) are dependent on small-scale magnetic active regions. Since flare energy is inversely proportional to event occurrence frequency, the measured flare properties for a given star are also dependent on observing depth and baseline. Our flare activity
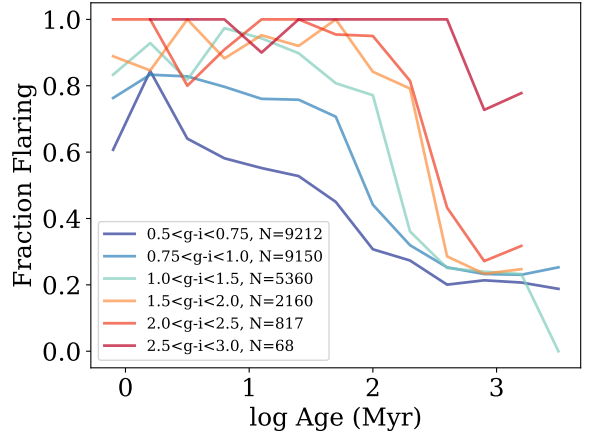

Figure 2. Fraction flaring stars as a function of their gyrochronology ages for 27,127 stars in six bins of $g - i$ color. The number of stars within each color bin is noted in the legend. Each star has a rotation period determined by McQuillan et al. (2014), and had artificial flare injection tests run by Davenport (2016b). Flaring stars were selected here as having at least 3 flare events above the 68% recovery completeness threshold in Davenport (2016b). We find a trend of increasing total fraction of active flare stars, and an increasing apparent lifetime for flare activity, with decreasing mass (redder stars).

metric must therefore represent the integrated properties of many individual flare events to accurately model a star's magnetic activity state.

In this section we outline three methods for quantifying the photometric flare activity between stars, as well as the merits and challenges of each approach. These metrics include: 1) the fractional energy emitted in the *Kepler* band by flares (L_{fl}/L_{Kp}), 2) the cumulative flare rate evaluated at a specific energy, and 3) an analytic model of the entire flare frequency distribution (FFD). While all three of these metrics have utility, we believe the latter will be of most value to future investigations, for example in studies of planetary habitability and atmosphere evolution.

We note that the pedagogical discussion here of comparing flare metrics between *Kepler* stars is similar in many ways to the review on flare activity by Kunkel (1975). This excellent review explored two different methods for quantifying and comparing flare activity from heterogeneous photometric studies: the integral of the light curve, and the rate at a given specific energy level, which are directly analogous to the first two approaches advanced here. The third approach, comparing the entire FFD between stars, has a long history (e.g. see Fig. 17 of Lacy et al. 1976), and has even been used for comparing *Kepler* flare stars (e.g. Ramsay et al. 2013; Hawley et al. 2014).

3.1. *Fractional Flare Luminosity*

An intuitive metric for quantifying magnetic activity strength via flares is the total luminosity emitted by flares relative to the nominal quiescent stellar luminosity, written originally as L_{fl}/L_{Kp} by Lurie et al. (2015). This quantity is inspired by traditional magnetic activity measures for low-mass stars, such as $L_{H\alpha}/L_{bol}$ (Walkowicz et al. 2004) or L_X/L_{bol} (Pallavicini et al. 1981), which are normalized relative to the bolometric stellar luminosity. In this case, as presented in Lurie et al. (2015), the flare luminosity is normalized to the quiescent luminosity of the star *only* in the *Kepler* bandpass. This metric was used by Davenport (2016b), and also recently by Yang et al. (2017).

The relative flare luminosity has many advantages as a magnetic activity strength indicator. First, it is algorithmically simple to compute by taking the integral of the flaring portion of the light curve, as described by Kunkel (1975). For *Kepler* light curves, this is done by de-trending the non-flaring (quiescent) light curves, including starspot variations, normalizing them to their average relative flux, and then integrating all the identified flares. Integrating the relative flux of a single flare results in a quantity known as the "equivalent duration"

(e.g. see Hunt-Walker et al. 2012), which has units of time (typically seconds). By integrating the relative flux from *all* flares in a *Kepler* light curve, we would again have units of time, and so as defined by Lurie et al. (2015) L_{fl}/L_{Kp} is simply computed as the integral of the relative flux of all flares, divided by the total observation duration of the light curve, resulting in a unit-less ratio.

A second appealing aspect of L_{fl}/L_{Kp} as a flare activity indicator is that it compresses the entire observed flare activity of a star, regardless of the duration of the observation window, into a single number. This results in a quantity that has higher signal-to-noise than a specific flare rate, for example. This makes L_{fl}/L_{Kp} ideal for comparing flare activity between stars, even with different observing baselines (e.g. comparing flare activity between active stars with differing numbers of quarters observed by *Kepler*).

Thirdly, the light curve data does not need to be flux calibrated, or have accurate distances determined to measure L_{fl}/L_{Kp}. Instead the metric is defined totally by the relative flux increases of the flares. This is especially useful for datasets like *Kepler*, where the light curves have incredible short-term precision designed to detect small amplitude exoplanet transits, but suffer from large-scale systematics that typically prevent flux calibration. As in the exoplanet transit application, the % change of the light curve is the only quantity required. This also results in L_{fl}/L_{Kp} being easily compared for many stars at once. Lurie et al. (2015), for example, used L_{fl}/L_{Kp} to measure flare activity for the M5+M5 binary system GJ 1245 AB, and to relate this flare activity to other mid-to-late type M dwarfs such as GJ 1243 (Davenport et al. 2014a).

As Lurie et al. (2015) note, to correctly compare flare activity between stars of varyings spectral types (or effective temperatures), the measured quantity L_{fl}/L_{Kp} requires a bolomet-
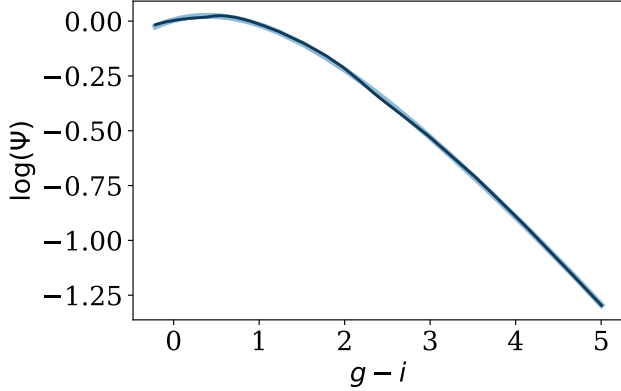
Figure 3. Flare Ψ, the correction factor (black line) that can be used to convert the observed fractional flare energy L_{fl}/L_{Kp} in to the metric for comparing between stars of different masses, L_{fl}/L_{bol}. This Ψ was computed using the bolometric and *Kepler* absolute magnitudes from a 600Myr PARSEC isochrone (Bressan et al. 2012). Here we show this correction factor versus $g - i$ color as a proxy for mass or spectral type (e.g. see Covey et al. 2007; Davenport et al. 2014b). A polynomial fit to the Ψ factor is also shown (blue line), and is described in the text below.

ric luminosity correction. Specifically, a correction must be made for the varying portion of the bolometric flux that is observed within the *Kepler* bandpass. This is akin to the "χ" parameter, first developed to convert Hα equivalent width measurements into $L_{H\alpha}/L_{bol}$, developed by Walkowicz et al. (2004). Douglas et al. (2014) recently produced a thorough discussion on developing a χ factor using model spectra, and produced an updated table of χ values as a function of photometric colors in many bands. We chose to use the letter Ψ as it follows χ in the Greek alphabet.

In Figure 3 we demonstrate a similar parameter that can be used for converting measured L_{fl}/L_{Kp} values into L_{fl}/L_{bol}, and thus more accurately compare the flare activity level between stars of different masses. The parameter Ψ was determined using the *Kepler* and bolometric luminosities computed for main sequence stars in

a 600 Myr isochrone from the PARSEC model grid Bressan et al. (2012). The very wide bandpass of the *Kepler* filter means the Ψ factor is relatively close to 1 for most stars, and doesn't change much between spectral types. For ease of use, we also provide a simple polynomial fit to the curve shown in Figure 3:

$$\log \Psi = -0.0013(g - i)^4 + 0.021(g - i)^3$$
$$-0.146(g - i)^2 + 0.105(g - i)$$
$$+0.004 \qquad (1)$$

Note that the Ψ parameter assumes a "gray" spectral response for the flare itself over the *Kepler* bandpass. While Hα emission occurs over a fairly small range of wavelength for most stars, flares emit energy over all observed wavelengths. The shape of this emission in optical wavelengths is typically characterized as a hot blackbody, usually with $T_{eff} \approx 10,000$ K, but has been seen to have significant excess emission in both the blue and red (e.g. see Kowalski et al. 2013). This effective temperature also changes throughout the flare event in a manner that is not well characterized, particularly for complex, multi-peaked flare events (e.g. Hawley & Pettersen 1991; Kowalski et al. 2012). Davenport (2016b) discussed this in terms of estimating the energy of a single flare event, assuming a gray flare response across the *Kepler* band. Some other studies assume a flare spectral model, which can in turn imply higher energies for specific events (e.g. Gizis et al. 2013; Maehara et al. 2015). The Ψ parameter shown in Figure 3 will similarly underestimate the flare luminosity. However, as in Davenport (2016b) we believe the best approach is to assume a gray response and not assume a single flare spectrum for all moments of every flare event.

Davenport (2016b) found that the fractional flare luminosity, L_{fl}/L_{Kp}, decreased with increasing Rossby number, which is defined as the rotation period divided by the convective turnover timescale (Ro = P$_{rot}/\tau$). This result
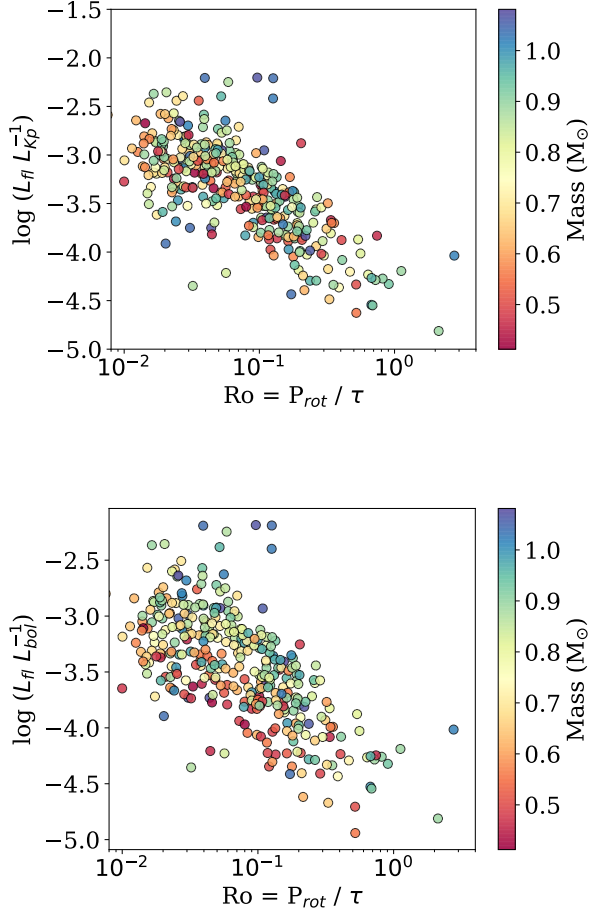
Figure 4. Rossby number vs flare energy for sample from Paper 1. Top: The original L_{fl}/L_{Kp} metric, as shown in Davenport (2016b) versus Rossby number, with points colored by the stellar masses estimated by Davenport (2016b) . Bottom: The new L_{fl}/L_{bol} metric, corrected using the Ψ parameter, with point colors as above.

indicates that the flare activity is decreasing with stellar age, as expected from other tracers of magnetic activity. In Figure 4 we reproduce the result of Davenport (2016b), coloring each point by the stellar mass. The lower panel of Figure 4 shows the Ψ corrected relative flare luminosity, L_{fl}/L_{bol}. Since the Ψ correction factor is near 1 for most stars, the change between these panels is modest. Interestingly, a gradient in the L_{fl}/L_{bol} as a function of mass appears for very rapidly rotating

stars, particularly those within the "saturated dynamo" regime (Ro < 0.1). The higher mass (near Solar mass) stars show a larger fraction of their luminosity emitted through flares in this regime. Though our sample of slower rotators is small, this gradient in L_{fl}/L_{bol} seems to disappear for larger Rossby numbers.

A final complication worth mentioning in the use of the relative flare luminosity metric is due to the varying distances and luminosities of stars in a given magnitude-limited sample. Since detection of flare events (particularly the small-amplitude, lower energy events) depends on the signal to noise of a light curve, the distances to stars can impact the resulting L_{fl}/L_{Kp} measurement. For example, given two identical mass stars with the same underlying flare activity level placed at different distances, the more distant star will have its smaller amplitude flares obscured by photometric noise, and thus a lower L_{fl}/L_{Kp}. Similarly, for two stars at a given distance, the lower-mass (fainter) one will have a lower signal-to-noise, and again the flare activity will be under-estimated. As a result, when comparing stars using L_{fl}/L_{Kp} (or L_{fl}/L_{bol}), a uniform range of flare event energies must be considered. This presents a major limitation in comparing the flare activity between stars of different masses. We therefore generally recommend L_{fl}/L_{Kp} be used when comparing between stars of similar mass.

3.2. *Specific Flare Rate*

Rather than integrating the relative flux from all detected flares within a light curve, as outlined in §3.1, flare activity can be expressed as a specific occurrence frequency. Since observable flares occur with a wide range of energies for a given star, such a frequency should be reported for flares of a given energy *or larger* (e.g. 10 flares per year with energies of 10^{32} erg or larger). This is equivalent to evaluating the flare frequency distribution (FFD; see Figure 1) at a given energy. Here we present this metric as

R_{32}, with the subscript denoting the log energy that rate is evaluated at, and with units of cumulative number per day.

The specific flare rate has been used in some capacity for many years for comparing flare activity levels between stars (e.g. Lacy et al. 1976), and was noted by Davenport (2016b) as an effective metric for comparing flare activity levels between stars at different distances. Since the specific flare rate is generated from the FFD, it can in principle be evaluated at energies *not* observed for a given star by fitting and extrapolating a powerlaw function to the FFD. Note this implicitly assumes that the flare rate for a star is governed by a single power law at all energies of interest, which is not always supported by observations. For example, as Davenport (2016b) highlight for KIC 11551430, a "break" in the FFD power law is observed for superflare stars at high event energies.

Projecting the specific flare rate using the single FFD power law very useful for comparing stars with different observing conditions, such as 1) stars with very different observing durations where one star may not have produced many large flares to compare to, or 2) comparing stars at significantly different distances where small amplitude flares from the fainter object are not detectable. What is required for projecting a flare rate to new energy range, however, is a sufficient number of flares be observed to adequately measure the power law distribution in the FFD.

This specific flare rate metric is also appealing due to its easily understood units, i.e. number of flares per day, and can be useful when considering the impact of flares on other observable properties. For example, Davenport (2016a) report for Proxima Cen a specific rate for superflares of $R_{33} = 8$ per year that may impact exoplanet habitability, and a rate of $R_{28} = 63$ per day for events having amplitudes comparable to an exoplanet transit signal.
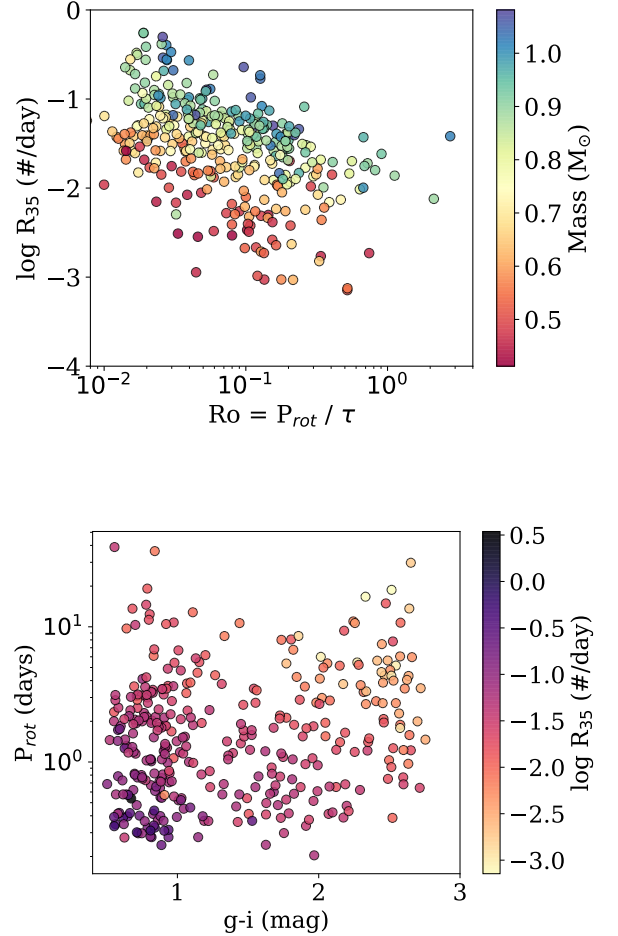

Figure 5. Specific flare rate (R_{35}), evaluated at an energy of log E = 35 erg as a function of the stellar mass and Rossby number (top), and the observed stellar rotation and color (bottom). The sample is the same as in Figure 4.

In Figure 5 we demonstrate the specific flare rate R_{35} for the same sample of stars shown in Figure 4. Here we explore both the dependence on mass and Rossby number (top) and the observed color and rotation period (bottom). The energy of 10^{35} erg was selected as the average event energy observed in the Davenport (2016b) flare census. For stars at a given mass or color the specific flare rate declines with increasing rotation period (or Rossby number), consistent with the results from the previous section. The specific flare rate is therefore a simple and ef-
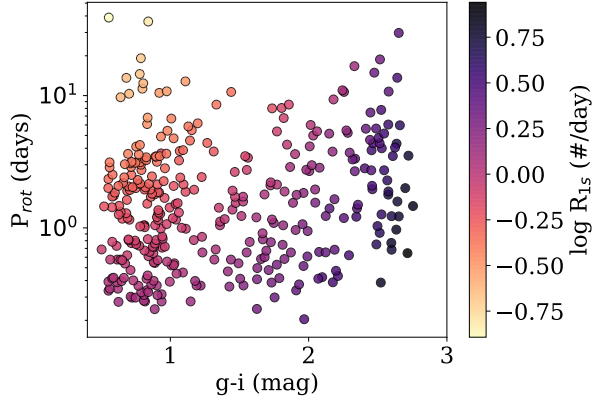
Figure 6. The Specific flare rate (R_{1s}), evaluated at an energy that is equal to an equivalent duration of 1 second

fective way to compare flare rates between stars at different distances and under vastly different observing conditions, provided the stars are comparable in color (mass).

However, a gradient in R_{35} in Figure 5 is seen as a function of both mass and color due to the specific flare rates being lower for low-mass stars at a given energy. The specific flare rate shows an unintuitive trend when comparing flare rates between stars of different masses, whereby lower-mass stars appear *less* active. This reproduces the previously known effect that while low-mass stars produce a high rate of observable flares and can produce a large fraction of their luminosity in flares, the actual rate of events with solar-type flare energies is low.

To overcome this unintuitive behavior, we can correct the specific flare rate for the difference in quiescent stellar luminosity between stars. Rather than pick a single event energy to evaluate all FFD's at, we instead pick a flare energy that scales with the star's luminosity. A flare event with an equivalent duration of $P = 1$ second by definition has an energy equal to the quiescent luminosity of the star integrated for 1 second. A sensible energy to choose for evaluating the FFD at therefore would be the star's

quiescent luminosity in the *Kepler* band[2]. We will denote this adjusted specific flare rate as R_{1s}, or literally the flare rate for events with an equivalent duration of 1 second. In Figure 6 we show the rotation–color space for the same sample of stars as a function of their R_{1s} specific flare rate. This adjusted specific flare rate exhibits the same decrease in flare activity with age (rotation), but is improved in that the low-mass stars display a higher flare activity level relative to their luminosity.

3.3. *Modeling the Flare Frequency Distribution*

The previous two metrics presented above have the useful property of reducing the complexity of the observed flaring behavior into a single quantity. While these are good approaches for easily comparing flare activity between stars (given certain caveats discussed above), such simple metrics neglect the important structure that is present in the full FFD (flare frequency distribution). Rather than try to fully reduce the complexity of the FFD down to a single number, here we demonstrate how to quantitatively use the full FFD to describe the evolution of stellar flare activity.

Comparing evolution of the entire FFD between stars requires considering a four dimensional space: cumulative flare frequency (the ordinate variable) as a function of flare event energy, stellar mass (or color), and age (or rotation period). Figure 7 shows the FFDs for our sample of NNN stars with measured rotation periods, separated into six bins based on their observed $g−i$ colors (as a proxy for mass). Each line shown is actually the mean FFD for a single star using all available quarters of *Kepler* data, the same as the average FFD shown in

---

[2] The bolometric luminosity would also be a good choice for defining the comparison energy, but as we explored in the development of the Ψ correction factor, the ratio of L_{Kp}/L_{bol} is typically near 1 for solar-type stars.
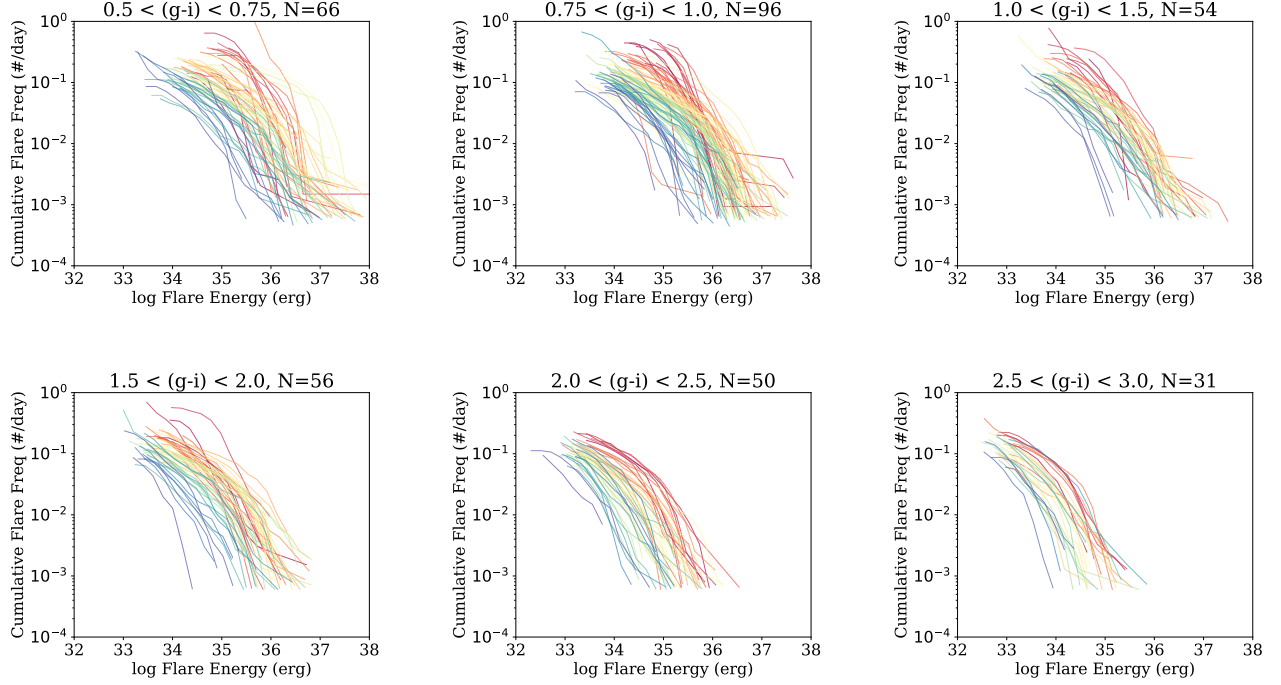
Figure 7. Average FFD, combining all available quarters of *Kepler* data, for stars in the 6 $g - i$ color bins defined in Davenport (2016b). Each track is colored as a function of the measured rotation period from McQuillan et al. (2014). A clear and coherent decrease in the total flare rates is observed as stars slow down (age) within each panel.

Figure 1. Each FFD line is colored by the observed rotation period reported by McQuillan et al. (2014), with increasing rotation periods from red to blue. Thus the panels of Figure 7 represent slices in mass of the four dimensional data space we are interested in.

The flare energy range observed within each panel of Figure 7 varies as a function of color bin, as expected from §3.2. The low-energy event cutoff for each star is determined by the automated flare injection and recovery tests described by Davenport (2016b). A bias is also seen where rapid rotators have slightly higher energy cutoffs due to increased starspot amplitudes that were not perfectly modeled out by `appaloosa`, which made flare recovery more difficult for the iterative algorithm of Davenport (2016b).

Another potential source of error in these FFDs come from the quiescent luminosities used to transform from the observed relative flare event "equivalent durations" into actual energies. Davenport (2016b) used the observed $g-i$ colors matched to a stellar isochrone to determine the distances and luminosities for each source. These estimates do not preclude binary stars or subgiants from contaminating our list of rotating stars. For example, Davenport (2017b) demonstrated using Gaia DR1 that a significant fraction of the nearest G dwarfs in the McQuillan et al. (2014) sample appeared to actually be subgiant contaminants. However, Gaia DR1 did not provide accurate distances to the entire Kepler sample, and so refining these distance estimates will have to wait for Gaia DR2. Regardless, we believe this energy zeropoint uncertainty will not significantly affect our analysis here, as we have limited ourselves to considering only the most flare-active stars from the Davenport (2016b) sample, and because each bin in

Figure 7 includes sources from a small range in stellar color.

A decrease in the observed flare frequency is seen as a function of rotation period in Figure 7 for every color bin, with flare rates monotonically deceasing as stars lose angular momentum. This is the evolution in flare activity we wish to model. Qualitatively the flare activity decreases more dramatically for the bluer stars, consistent with results from e.g. Figure 6, and our expectations from other measures of stellar magnetic activity over time (e.g. Shkolnik & Barman 2014). As Davenport (2016b) noted for a single flaring G dwarf, a "break" in the FFD power law is apparent at the highest flare event energies. This break energy also seems to scale with observed energy range of events within each $g - i$ color bin (i.e. lower-mass stars have a lower break energy). Though we do not fully explore this feature here, we emphasize that it may represent an important limit on the energy budget of stellar active region formation as a function of the total stellar magnetic field strength (i.e. over time).

To produce a model for the FFD with the most utility for follow-up studies, we convert the colors and periods for each star in our sample into masses and ages, respectively. The $g - i$ color for each star was converted to stellar mass using a 600 Myr isochrone, as described in Davenport (2016b). Similarly, producing an age for each star requires adopting a "gyrochrone" (gyrochronology isochrone) model prescription. Considerable effort has been made to explore the accuracy of such models for main sequence stars at a range of ages in the *Kepler* era (e.g. Meibom et al. 2011; Angus et al. 2015; Douglas et al. 2016). Most models produce similar age–rotation estimates for stars between roughly 500 Myr and a few Gyr. However, significant problems appear to exist for older, slower rotators, where a break in the angular momentum loss mechanism results in old stars (Solar age and

older) with anomalously fast rotation periods (van Saders et al. 2016). As our sample of flare stars is biased towards the more active, younger main sequence stars, and so we do not expect this spin-down break to affect our results. Our ages come from the Mamajek & Hillenbrand (2008) gyrochrone model. While future gyrochronology models are likely to produce more accurate ages, we believe this model will give an appropriate distribution of ages as a function of the observed rotation period and stellar color.

To model the time dependent FFD we have adopted a power law decrease in the flare activity rate over time. Our chosen parameterization is supported by other observations of the decline in other magnetic activity indicators over stellar age, included the fractional flare luminosity discussed in §3.1. Specifically we have used the following model to fit the FFDs of all stars in our sample simultaneously:

$$\log \nu = a \log \varepsilon + b \tag{2}$$
$$a = a_1 \log t + a_2 m + a_3$$
$$b = b_1 \log t + b_2 m + b_3$$

Note the first part of this equation is simply the definition of the FFD power law distribution for the reverse cumulative number of flares per day (ν) as a function of flare event energy in erg (ε), written to take the form of a linear equation in log-log space. We then add terms to the coefficients a and b that include linear dependence on the log of the stellar age (t, in Myr), as well as the stellar mass (m, relative to solar).

We explored other parameterizations of this FFD evolution model, including additional cross terms as a function of mass and age, e.g. $a_4(m \times \log t)$. The Bayesian Information Criterion (BIC) did not yield a significant increase in the quality of the fit to the data given these extra degrees of freedom. Further, we currently have no theoretical basis for using a more com-

plicated model for flare evolution as a function of time or mass. The possible break in the FFD power law for large energy flares, noted by Davenport (2016b) and in our Figure 1, was not included in our parameterization of Equation 2. Instead we focus on reproducing the single dominant power law FFD relationship, which has been reported to characterize the distribution of flares on the Sun and solar-type stars over more than 10 orders of magnitude in event energy (e.g. Fig. 9 from Shibayama et al. 2013). We also did not attempt to include the "saturated" activity regime, suggested by Davenport (2016b) for rapidly rotating stars with Rossby numbers lower than ∼0.03, in our FFD model. As Davenport (2016b) notes, the break does not occur at the same Rossby number as other magnetic activity indicators (typically Ro=0.1) and the support for this break in the *Kepler* flare data is currently tenuous. Exploring these additional model parameters is not technically difficult, but additional flare stars from missions like K2 and TESS are needed to determine if they are necessary.

Our model fitting in `Python` required an array containing all of the stellar ages in $\log(t/\text{Myr})$ and masses (in units of Solar mass), and all flare event energies in $\log(\varepsilon/\text{ erg})$, and produced the cumulative flare rate in $\log(\nu/day)$ for each star. Uncertainties in the flare rate were included in our fit, using the Poisson event counting uncertainty approximation from Equation 12 of Gehrels (1986). No errors for the flare energies, or in our mass and age estimates were used in the fit. The model in Equation 2 was fit to the entire flare star sample using an error weighted least-squares minimization to generate an initial guess for the six free parameters.

The initial fit for Equation 2 was then refined using the Affine Invariant Markov Chain Monte Carlo (MCMC) ensemble sampler, `emcee` (Foreman-Mackey et al. 2013). We first ran `emcee` for a "burn-in" phase of 500 steps us-

Table 1. Median parameters for the FFD evolution model described in Equation 2 found from our MCMC exploration.

$a_1 = -0.07$	$a_2 = 0.79$	$a_3 = -1.06$
$b_1 = 2.01$	$b_2 = -25.15$	$b_3 = 33.99$

ing 100 walkers, seeded around the initial least-squares solution. The sampler was then run for 100,000 steps to explore parameter space. The MCMC chains were well converged for all 6 free parameters after the 100,000-step run, having an autocorrelation time of ∼60 steps for each parameter. The final coefficients used for our FFD evolution model were determined using the median of the converged portion of the MCMC chains, and are given in Table 1. In Figure 8 we also present the standard `corner` plot (Foreman-Mackey 2016), which shows the 1- and 2-dimensional posterior distributions for each free parameter for Equation 2 from the MCMC sampler.

The 2-dimensional posterior distributions shown in Figure 8 demonstrate that degeneracies are apparent between several parameters in our model. These can be identified as very narrow distributions in three panels of the panels from Figure 8: (a_1, b_1), (a_2, b_2), and (a_3, b_3). This can be interpreted as indicating that the model adopted in in Equation 2 has unnecessary complexity, or that perhaps it could be re-cast into a more fundamental parameter space. As noted above, we have chosen the FFD evolution model in Equation 2 for ease of implementation, and for lack of a better theoretical basis. The posterior distributions shown in Figure 8 make it clear that other parameterizations should be explored in future studies.

In Figure 9 we demonstrate our FFD evolution model's ability to reproduce the observed FFDs for several stars. Here we show the combined FFD for the same three flare stars as in Figure 1, but with the predicted FFD from Equation 2 overlaid. As discussed previously, we do not at-
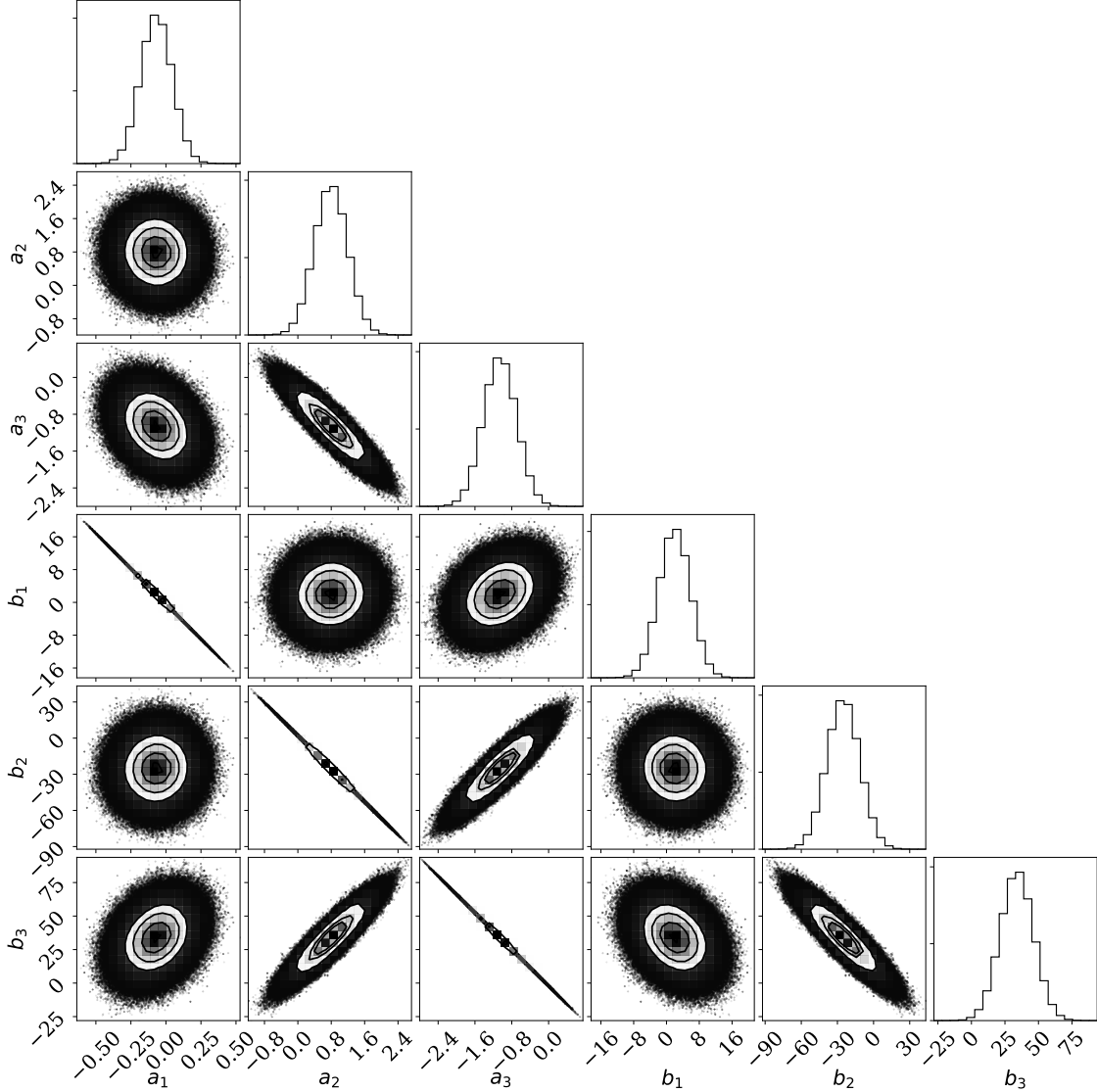
Figure 8. The standard MCMC sampler result `corner` plot, showing the 1- and 2-dimensional posterior distributions for each free parameter in Eqn. 2. The density of points and contours correlate with the posterior probability distribution from a 100,000-step run of the `emcee` sampler. Degeneracies are apparent between several parameters, seen here as very narrow distributions in three panels (a_1, b_1), (a_2, b_2), and (a_3, b_3), indicating our chosen model in Eqn. 2 may have unnecessary complexity.

tempt to model any break in the FFD slope at high flare energies. The model reproduces the specific flare rates for each stars well, as well as the dominant slopes for the FFDs. These examples represent the ability of our flare evolution model to describe the FFD for a low-mass star at a given mass and age, and we anticipate this model will be helpful for future studies of the

flare activity, such as exoplanet host evolution, or updating the predicted flare yields from surveys like LSST (Najita et al. 2016).

Finally in this section, we briefly note our lack of including null detections in this analysis. While our sample analyzed for the FFD evolution contains 347 stars, there were nearly two orders of magnitude more stars with good col-
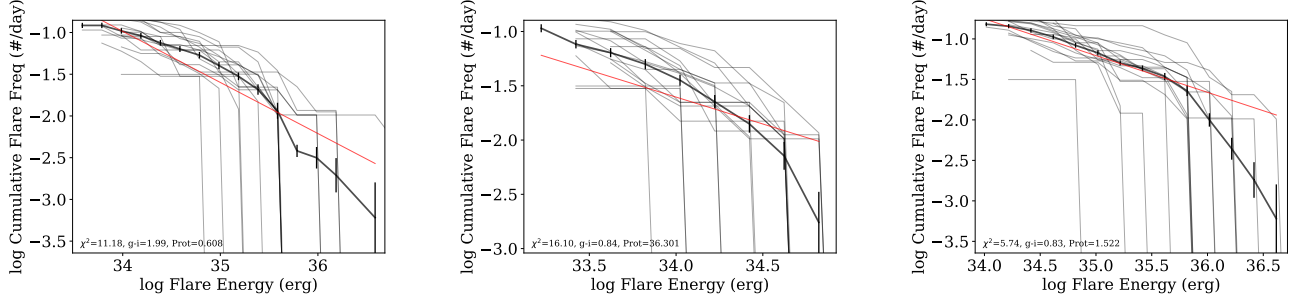
Figure 9. Flare frequency distributions as shown from Figure 1 (black line), but with the final flare activity model from Equation 2 evaluated for each star's mass and age (red line). Note this model was not fit for each star's FFD individually, but instead was fit to our entire sample.

ors (and therefore mass estimates) from Davenport (2016b) and rotation periods from McQuillan et al. (2014). The flare injection tests from Davenport (2016b) do also provide conservative estimates of the lowest energy flare that could have been detected in each object's *Kepler* light curve with `appaloosa`. We experimented with including these null detections in our model fitting as upper limits, using an observed flare rate of zero, and an uncertainty on the flare rate of 1 event per the total duration of observation (∼4 years for most targets). However, we found two practical challenges that prevented us from using these targets in our model fitting: 1) it was not clear over what energy range in the FFD this upper limit should be considered for each object, and 2) these upper limits dominated the sample, and thus drove the model fitting to systematically under-predict the flare rates observed in our entire "good" sample of 347 stars.

4. EXPLORING THE FLARE RATE EVOLUTION

Using our FFD evolution model trained on a sparse sample of field stars with varying masses and ages, we can explore how a single star evolves over its lifetime. In Figure 10 we show the FFD for a theoretical 0.5 M$_\odot$ star (approximately an M0 dwarf), and for a 1 M$_\odot$ star, both evaluated at four logarithmically spaced

ages from 10 Myr to 1 Gyr. The solar-mass star has a specific flare rate that decreases more rapidly than the model M dwarf. A very small change in the FFD slope is seen for the M dwarf, with the FFD getting steeper (fewer large flares) over time. However, given the small number of M dwarfs in our sample with old ages, the reliability of this change in slope is questionable. We find the FFD slope is effectively constant for stars at all ages.

Extending the FFD for a theoretical solar-mass star to the age of the Sun (here assumed to be 4.6 Gyr), we find our model over-predicts the rate of superflares determined for "average Sun-like stars" in *Kepler* by Shibayama et al. (2013). Instead, our model closely fits their "most active Sun-like" sample. We believe this is due to our sample having insufficient numbers of slowly rotating G dwarfs to accurately predict the behavior of older stars. We also note a potential Malmquist-like bias in our flare rate determination exists due the possible existence of activity cycles. As Shibayama et al. (2013) and Clarke et al. (2018) note, flare activity might vary by an order of magnitude on these stars over their activity cycles (see also Veronig et al. 2002), and so our sample may preferentially include stars near their highest activity states.

Our FFD evolution model can also be used to predict *other* flare activity metrics described in this paper. For example, in Figure 11 we com-
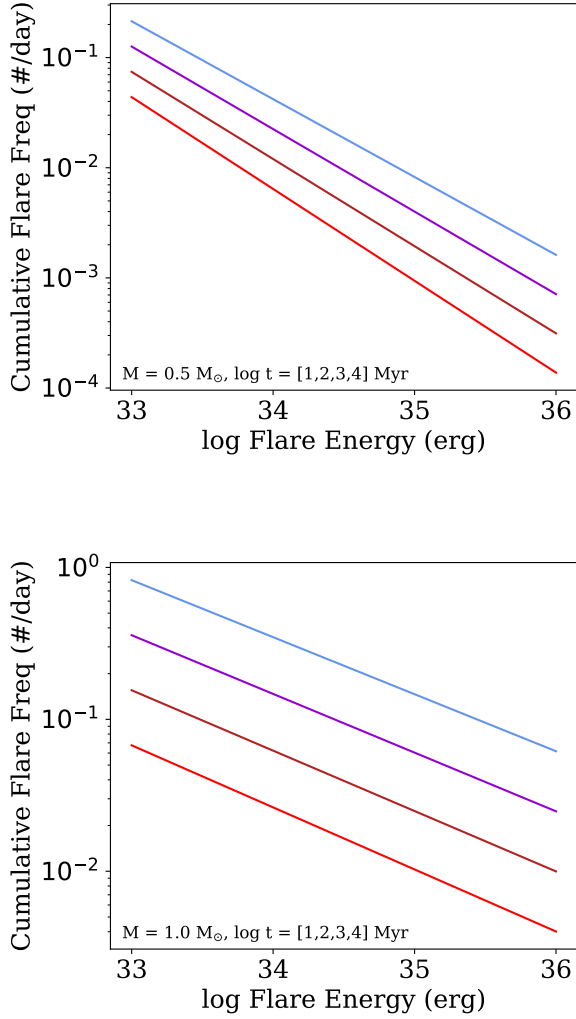
Figure 10. Our best-fit flare evolution model showing the predicted FFD evaluated at four age bins for a $0.5 M_\odot$ (top) and $1.0 M_\odot$ star (bottom). While the change in FFD slopes as a function of age is negligible, the difference as a function of mass is significant. Note: These FFDs are drawn at the same energy ranges for ease of comparison, but do not correspond to the specific flare energies detected at these masses.

pute R_{35}, the specific flare rate at an energy of $\log \varepsilon = 35$ erg, and with our metric of R_{1s} developed in §3.2 that scales with the quiescent luminosity of the star. The specific flare rate here is determined by evaluating the FFD at a given energy over a dense grid of ages and masses, al-
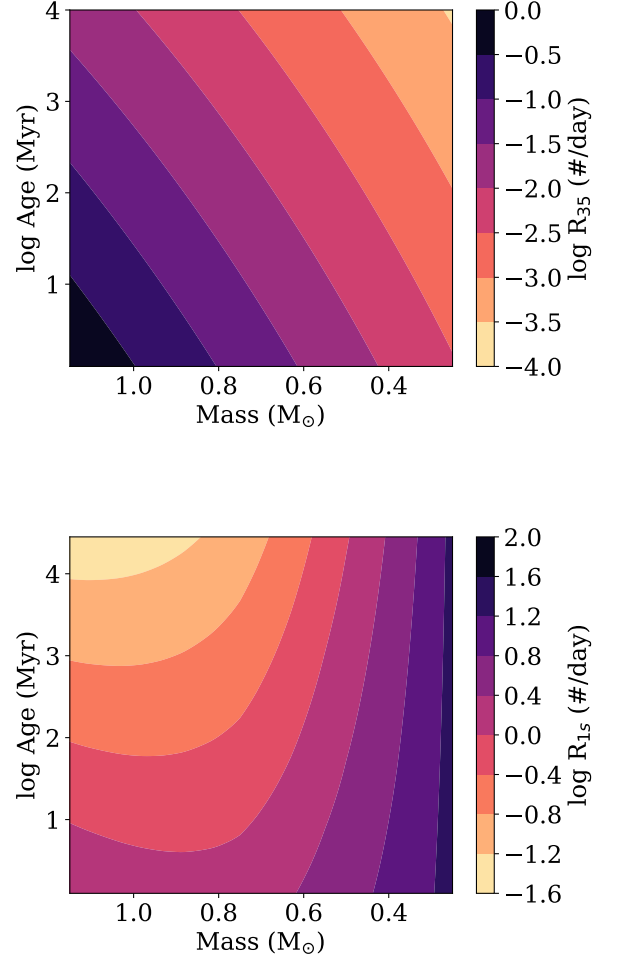
Figure 11. Our best-fit FFD evolution model evaluated over a grid of masses and ages, showing the cumulative flare rate R_{35} for a fixed energy of 10^{35} erg (top), and at an equivalent duration of 1 second, i.e. $R_{1s} = 1 \sec \times L_{quies}$ (bottom). The latter clearly shows that low-mass stars produce more flares relative to their quiescent luminosity, while all stars show a decrease in their specific flare rate over time.

lowing us to draw this phenomenological surface of flare activity as a function of mass and age. As noted in §3.2, R_{1s} broadly shows the more intuitive behavior that low-mass stars have flare activity that declines more slowly with age.

Computing the fractional flare luminosity, L_{fl}/L_{Kp}, using our FFD evolution model is more subtle due to the considerations described

in §3.1. For example, the energy range of flare events to model the FFD over must be chosen at every age and mass. To match observations it is important to pick an energy range of flares that scales with each star's quiescent luminosity. The fractional flare luminosity was computed using a preliminary version of our FFD evolution model for Clarke et al. (2018), which examined the change in L_{fl}/L_{Kp} between stars of varying mass ratios over a 1 Gyr timespan. This was computed at each age by integrating the FFD over six orders of magnitude in flare event energy, a larger dynamic range of events than typically observed for stars in *Kepler*, even very active stars like GJ 1243 (Hawley et al. 2014). However, the same range of energies was used for both stars, regardless of the mass ratio considered. Clarke et al. (2018) found that the ratio of L_{fl}/L_{Kp} between stars was roughly constant over time (up to 1 Gyr), which is again due to the model FFD slope remaining effectively the same at all ages for a given star.

5. DISCUSSION AND SUMMARY

Here we have presented a thorough discussion of three methods for quantifying and comparing the flare activity of stars from optical light curves. Each method has advantages and disadvantages in terms of ease of implementation and computation, robustness to incomplete or low signal-to-noise data, and in the ability compare between stars of varying masses and distances. The specific flare rate and the fractional flare luminosity are recommended for applications needing a simple, single metric, while modeling the entire flare frequency distribution (FFD) is preferred for accurately describing the details of a single, well studied flare star.

In the development of the fractional flare luminosity, we have also introduced the "Ψ factor". This quantity was described first by Lurie et al. (2015) as a bolometric correction for the fractional flare luminosity observed in a given passband, and has been demonstrated here for

the *Kepler* band using an isochrone to estimate the bolometric luminosity. Since the *Kepler* band cover a wide range of the optical regime, this correction is fairly insignificant for correcting flare activity in this sample. However, such an approach will be critical for comparing the flare activity between observations from various traditional optical bands (e.g. U-, B-, and V-bands).

In our ensemble modeling of the FFD, we have assumed a simple parameterization to continuously describe the evolution of flare activity as a function of both stellar mass and age (Eqn. 2). This model is a simple extension of the FFD power law commonly observed, with extra terms added for log(age) and mass. We have pointed out several aspects of FFD that have not been described by this model, including the potential break in the power law at high event energies, as well as regime of saturated activity for rapidly rotating (young) stars. As the sample of robust flare stars from *Kepler*, K2, and soon TESS grows, the parameterization of the FFD evolution model should be revisited, with these features added a additional free parameters. The axes of this model should also be reexamined, such as parametrizing the evolution in terms of Rossby number rather than age.

We find the FFD slope does not significantly change for stars as a function of their age. This suggests our FFD evolution model could be simplified in the future by keeping the slope fixed. This result also has potentially deep meaning for the physics of flares, indicating for example the same rules of self-organized criticality are at work regardless of the star's total magnetic field strength. It is not clear from our work at this time, however, over what energy range this slope is applicable, nor how that energy range changes with stellar age. Unfortunately *Kepler*'s red wavelength coverage makes detecting very small energy flares difficult, and so it is

not clear if this single power law slope extends far enough down in energy to be an important component of support for the lower stellar atmosphere (e.g. "Ellerman Bombs"; Hansteen et al. 2017). However, if the nano/micro-flare rate evolves coherently with the larger events and super-flare rates observed here (i.e. if the power law is preserved to very low energy events), this atmospheric support mechanism must change as the total flare rate decreases. Otherwise the lower stellar atmosphere support would decrease, and the stellar radius could change over time.

Finally we note that all temporal evolution implied in this work relies on the assumption that gyrochronology accurately sorts stars as as a function of their age. This neglects, for example, any dynamical evolution in binaries that can affect the present day rotation (e.g. Lurie et al. 2017; Clarke et al. 2018). We have also not utilized the stellar open clusters available in the *Kepler* field, which are ideal benchmarks for stars at fixed ages. The sample of flare stars found in these clusters in *Kepler* is too small to be used for a statistical analysis. However, with a number of nearby young clusters available in K2, future work should focus on comparing the flare activity between stars of known ages.

REFERENCES

Ambartsumian, V. A., & Mirzoian, L. V. 1975, in IAU Symposium, Vol. 67, Variable Stars and Stellar Evolution, ed. V. E. Sherwood & L. Plaut, 3–14

Angus, R., Aigrain, S., Foreman-Mackey, D., & McQuillan, A. 2015, MNRAS, 450, 1787

Balona, L. A. 2012, MNRAS, 423, 3420

Borucki, W. J., Koch, D., Basri, G., et al. 2010, Science, 327, 977

Bressan, A., Marigo, P., Girardi, L., et al. 2012, MNRAS, 427, 127

Candelaresi, S., Hillier, A., Maehara, H., Brandenburg, A., & Shibata, K. 2014, ArXiv e-prints 1405.1453, arXiv:1405.1453

Clarke, R. W., Davenport, J. R. A., Covey, K. R., & Baranec, C. 2018, ApJ, 853, 59

Covey, K. R., Ivezić, Ž., Schlegel, D., et al. 2007, AJ, 134, 2398

Davenport, J. R. A. 2016a, ArXiv e-prints, arXiv:1610.08563

—. 2016b, ApJ, 829, 23

—. 2017a, Research Notes of the American Astronomical Society, 1, 2

—. 2017b, ApJ, 835, 16

Davenport, J. R. A., Hawley, S. L., Hebb, L., et al. 2014a, ApJ, 797, 122

Davenport, J. R. A., Ivezić, Ž., Becker, A. C., et al. 2014b, MNRAS, 440, 3430

Douglas, S. T., Agüeros, M. A., Covey, K. R., et al. 2016, ApJ, 822, 47

—. 2014, ApJ, 795, 161

Feigelson, E. D. 2001, in Astronomical Society of the Pacific Conference Series, Vol. 248, Magnetic Fields Across the Hertzsprung-Russell Diagram, ed. G. Mathys, S. K. Solanki, & D. T. Wickramasinghe, 495

Foreman-Mackey, D. 2016, The Journal of Open Source Software, 24, doi:10.21105/joss.00024

Foreman-Mackey, D., Hogg, D. W., Lang, D., & Goodman, J. 2013, PASP, 125, 306

Gehrels, N. 1986, ApJ, 303, 336

Gizis, J. E., Burgasser, A. J., Berger, E., et al. 2013, ApJ, 779, 172

Hansteen, V. H., Archontis, V., Pereira, T. M. D., et al. 2017, ApJ, 839, 22

Haro, G., & Chavira, E. 1966, Vistas in Astronomy, 8, 89

Hawley, S. L., Davenport, J. R. A., Kowalski, A. F., et al. 2014, ApJ, 797, 121

Hawley, S. L., & Pettersen, B. R. 1991, ApJ, 378, 725

Hilton, E. J., West, A. A., Hawley, S. L., & Kowalski, A. F. 2010, AJ, 140, 1402

Hunt-Walker, N. M., Hilton, E. J., Kowalski, A. F., Hawley, S. L., & Matthews, J. M. 2012, PASP, 124, 545

Kipping, D. M., Cameron, C., Hartman, J. D., et al. 2017, AJ, 153, 93

Kowalski, A. F., Hawley, S. L., Hilton, E. J., et al. 2009, AJ, 138, 633

Kowalski, A. F., Hawley, S. L., Holtzman, J. A., Wisniewski, J. P., & Hilton, E. J. 2012, SoPh, 277, 21

Kowalski, A. F., Hawley, S. L., Wisniewski, J. P., et al. 2013, ApJS, 207, 15

Kunkel, W. E. 1975, in IAU Symposium, Vol. 67, Variable Stars and Stellar Evolution, ed. V. E. Sherwood & L. Plaut, 15–46

Lacy, C. H., Moffett, T. J., & Evans, D. S. 1976, ApJS, 30, 85

Luger, R., Barnes, R., Lopez, E., et al. 2015, Astrobiology, 15, 57

Lurie, J. C., Davenport, J. R. A., Hawley, S. L., et al. 2015, ApJ, 800, 95

Lurie, J. C., Vyhmeister, K., Hawley, S. L., et al. 2017, AJ, 154, 250

Maehara, H., Shibayama, T., Notsu, Y., et al. 2015, Earth, Planets, and Space, 67, 59

Mamajek, E. E., & Hillenbrand, L. A. 2008, ApJ, 687, 1264

McQuillan, A., Mazeh, T., & Aigrain, S. 2014, ApJS, 211, 24

Meibom, S., Mathieu, R. D., Stassun, K. G., Liebesny, P., & Saar, S. H. 2011, ApJ, 733, 115

Najita, J., Willman, B., Finkbeiner, D. P., et al. 2016, ArXiv e-prints, arXiv:1610.01661

Pallavicini, R., Golub, L., Rosner, R., et al. 1981, ApJ, 248, 279

Ramsay, G., Doyle, J. G., Hakala, P., et al. 2013, MNRAS, 434, 2451

Segura, A., Walkowicz, L. M., Meadows, V., Kasting, J., & Hawley, S. 2010, Astrobiology, 10, 751

Shibayama, T., Maehara, H., Notsu, S., et al. 2013, ApJS, 209, 5

Shkolnik, E. L., & Barman, T. S. 2014, AJ, 148, 64

Skumanich, A. 1972, ApJ, 171, 565

—. 1986, ApJ, 309, 858

Tilley, M. A., Segura, A., Meadows, V. S., Hawley, S., & Davenport, J. 2017, ArXiv e-prints, arXiv:1711.08484

Van Doorsselaere, T., Shariati, H., & Debosscher, J. 2017, ApJS, 232, 26

van Saders, J. L., Ceillier, T., Metcalfe, T. S., et al. 2016, Nature, 529, 181

van Saders, J. L., Pinsonneault, M. H., & Barbieri, M. 2018, ArXiv e-prints, arXiv:1803.04971

Veronig, A., Temmer, M., Hanslmeier, A., Otruba, W., & Messerotti, M. 2002, A&A, 382, 1070

Vidotto, A. A., Gregory, S. G., Jardine, M., et al. 2014, MNRAS, 441, 2361

Walkowicz, L. M., Hawley, S. L., & West, A. A. 2004, PASP, 116, 1105

Walkowicz, L. M., Basri, G., Batalha, N., et al. 2011, AJ, 141, 50

West, A. A., Hawley, S. L., Bochanski, J. J., et al. 2008, AJ, 135, 785

West, A. A., Weisenburger, K. L., Irwin, J., et al. 2015, ApJ, 812, 3

Wright, N. J., Drake, J. J., Mamajek, E. E., & Henry, G. W. 2011, ApJ, 743, 48

Yang, H., Liu, J., Gao, Q., et al. 2017, ApJ, 849, 36